Fe^+ ion irradiation effects in Fe-10at%Cr films irradiated at 300 °C

S. Pantousa[1,2], K. Mergia[1], A. Ionescu[3], E. Manios[1], S. Dellis[1], C. Kinane[4], S. Langridge[4], A. Caruana[4], U. Kentsch[5], and S. Messoloras[1]

[1] Institute of Nuclear and Radiological Sciences and Technology, Energy and Safety, NCSR "Demokritos", Athens, 15341, Greece
[2] Department of Physics, School of Sciences, University of Athens, Athens, 15772, Greece
[3] Cavendish Laboratory, University of Cambridge, J J Thomson Avenue 19, Cambridge CB3 0HE, UK
[4] ISIS neutron and muon source, Rutherford Appleton Laboratory, United Kingdom
[5] Ion Beam Center, Helmholtz-Zentrum Dresden-Rossendorf, Germany

Abstract

Fe-Cr alloys constitute the model systems for the investigation of radiation damage effects in ferritic-martensitic steels which are candidate structural materials for fusion reactors. In the current study Fe-10at%Cr alloy films of 70 nm thickness were irradiated by 490 keV Fe+ ions at 300 °C at doses ranging from 0.5 up to 20 displacements per atom (dpa). The Fe+ ion energy chosen corresponds to the energy of primary Fe(Cr) knock-on atoms from 14 MeV neutrons. The irradiation effects were investigated employing X-ray diffraction and X-ray and polarized neutron reflectivity. The irradiation produced dose dependent: a) lattice constant increase, b) grain size growth and c) Cr depletion in the matrix. These changes occur largely up to 4 dpa and afterwards the system attains a dynamic equilibrium.

Keywords: Fe-Cr alloys, ion irradiation, lattice damage, Cr depletion, polarized neutron reflectivity, magnetization.

1. Introduction

Ferritic–martensitic (F-M) steels are the leading candidate structural materials for fusion power plants [1], [2], [3]. The role of Cr is critical regarding the properties of F-M steels, for example addition of only 2% Cr to pure Fe results in drastic radiation – induced swelling suppression [4]. Alloys with Cr percentage of about 10 at% are the choice for fusion energy applications as they present low Ductile to Brittle Transition Temperature (DBTT), high swelling resistance due to their long cavity incubation time [5], [6], [7] and corrosion resistance [8]. There is a large number of experimental studies of the radiation induced effects in the microstructure and mechanical properties of such alloys as for example [9], [10], [11], [12], [13], and references therein. Theoretical work has demonstrated that magnetic structure is an important feature in understanding the radiation effects [14], [15] and it has been demonstrated that self-ion irradiation induces drastic changes in the magnetic properties of polycrystalline Fe(Cr) films [16], [17], [18].

Improvement of F-M steels to withstand the fusion environment of high temperatures and the damage induced by energetic neutrons requires the in-depth understanding of the underlying physics and utilization of thus acquired knowledge in predictive modelling of the materials performance. For this purpose, investigation of the properties of Fe-Cr alloys, as the generic alloy of F-M steels, under temperature and irradiation is a suitable route.

Neutrons produced by the deuterium-tritium reaction have a kinetic energy of 14.1 MeV, however, the neutron spectrum in the First Wall and Blanket is of small variation or almost flat, respectively, in the energy region from 0.1 keV to 1 MeV [19]. The neutron irradiation effects arise from the generation of primary knock-on atoms (PKAs) of different energies and transmutation products. The consequences of the PKAs on the material properties can be evaluated by self-ion irradiations. Ion irradiation presents a number of advantages as well-defined energies, fluxes and temperature and the possibility to study high doses in reduced times [20]. It also offers the possibility either to exclude transmutation production effects and focus the investigation on atomic displacement in order to enhance basic knowledge understanding and assist model validation or to study synergetic effects using double or triple beam irradiations. The mean energy of Fe PKA from the 14 MeV neutrons is around 490 keV and this energy was chosen in a series of Fe+ ion irradiations of Fe(Cr) [16],[17],[18]. Also, it has been shown that around this energy occurs the maximum displacement per atom (dpa) per year in pure iron in the first wall for a conceptual design of a demonstration fusion power plant [21].

Previous experimental investigations showed that 490 keV Fe+ ion irradiation on Fe-10at%Cr at room temperature results in an increase of the Fe-Cr magnetization as the radiation damage increases and this was attributed to the Cr depletion from the Fe-Cr matrix [18]. In the present work the investigation of 490 keV Fe+ ion irradiation effects on Fe-10at%Cr is extended at the irradiation temperature of 300 °C. The irradiation temperature of 300 °C is chosen because it lies within the service temperature range of the water-cooled blanket option for DEMO fusion

reactor [22]. Fe-10at%Cr alloys in the form of films with thickness of 70 nm are investigated in the dose range from 0.5 to 20 dpa.

2. Materials and experimental methods

2.1. Sample specifications

As the ions have limited penetration range, the most appropriate sample form material for ion irradiations is that of a thin film. In order to avoid blending ion implantation effects with atomic displacement effects, the film thickness has to be chosen carefully. The recoiling iron and chromium atoms and the implantation probability of the Fe+ ions per incident ion, as they resulted from simulations using the software SRIM-2013 [23], are presented as a function of depth of the Fe-10at%Cr film in **Figure 1**(a). A Full – Cascade SRIM calculation was performed with the displacement energy, E_d, for iron and chromium set to 40 eV (ASTM standard, [24]) and the lattice binding energy, E_b, set equal to zero for both target atoms [25]. The maximum penetration depth of the 490 keV ions was found to be around 400 nm. The implantation probability presents a Gaussian distribution (solid line in **Figure 1**(a)) with a maximum at about 180 nm while the recoils present a maximum around 120 nm. For the chosen film thickness of 70 nm the radiation damage effects are predominant, while the implantation effects are minimized. The total implanted Fe atoms in the whole film thickness of 70 nm for the maximum dose of 20 dpa is about 0.1 at%, thus the Cr concentration of the Fe-Cr alloy is not affected by the implantation effects.

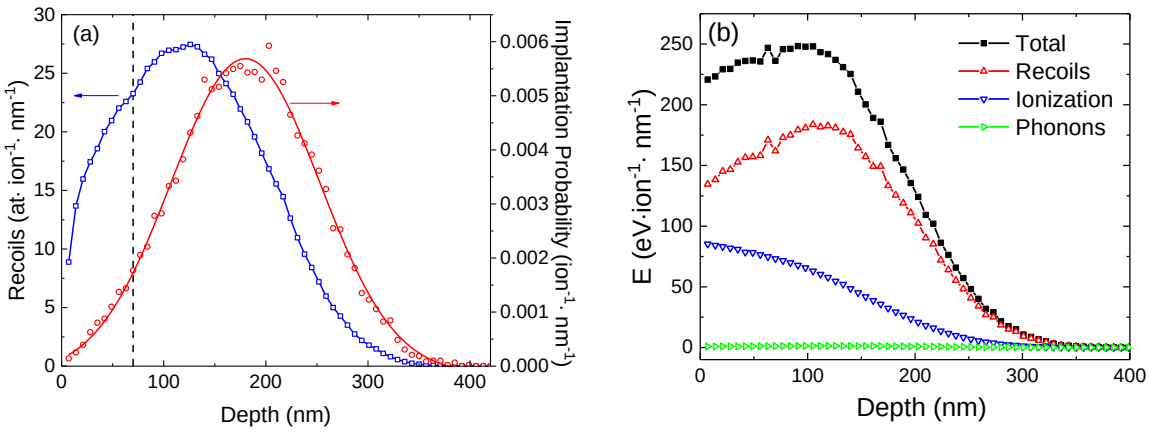

Figure 1: SRIM calculations for 490 keV Fe+ ions on Fe-10at%Cr. The vertical dashed line at 70 nm in (a) indicates the thickness of the films used in this study. (a) Recoils and implantation probability as a function of depth. The solid line for the implantation probability is a Gaussian fit. (b) Energy deposited to recoils, electron ionization and phonons as a function of depth.

Another important aspect in simplifying the premises of the understanding of radiation damage is the energy deposited in the lattice. We observe in **Figure 1**(b) that the total deposited energy for up to 140 nm depth is almost constant and around 230 $eV \cdot ion^{-1} \cdot nm^{-1}$. Thus the incident Fe+ ion after it passes a film having a thickness of 70 nm loses an energy of around 16 keV which is negligible compared to its initial energy of 490 keV, thus for the whole film thickness the incident Fe+ ion has almost constant energy. Therefore, by using an FeCr film of 70 nm thickness we succeed in having homogeneous irradiation conditions which simplifies understanding and subsequent modelling of the irradiation effects.

2.2. Fe-Cr thin films fabrication and characterization

Fe-10at%Cr films with thickness of 70 nm were fabricated on 10×10 mm Si/SiO_2(300nm) substrates employing DC magnetron sputtering. On top of the Fe-Cr films a thin layer of Cr, of around 5 nm thickness, has been deposited in order to prevent the oxidation of the films. The deposition took place at room temperature in a high vacuum chamber with a base pressure $<3\times10^{-8}$ mbar and simultaneously for all the films. High purity Fe-10at%Cr (99.99%) and Cr (99.95%) targets were used and the deposition rate was 0.191 Å/s and 0.214 Å/s for the Fe-Cr and the Cr layer, respectively. The films were fabricated at the Materials Growth Facility (MGF) in the Cavendish Laboratory of the University of Cambridge.

2.3. Fe+ ion irradiations

The Fe+ irradiations were performed at the 500 kV air insulated accelerator made by HVEE of the Ion Beam Center in HZDR in Dresden, Germany. The Fe-10at%Cr films were irradiated at 300 °C with 490 keV Fe+ ions, at doses ranging from 0.5 (2.3×10^{14} ions/cm^2,) to 20 dpa (9.2×10^{15} ions/cm^2) with a flux of 10^{12} ions/cm^2/s and at the dose rate of 0.002 dpa/s. The time required for achieving 1 dpa damage is around 8 min. The samples were placed under high vacuum (10^{-7} – 10^{-6} mbar) and the temperature was controlled through a K-type thermocouple attached on the sample holder. The surface temperature of the irradiated films was monitored with a calibrated infrared camera. The ion beam was incident at 7° with respect to the sample normal in order to prevent any ion channeling.

2.4. X-ray diffraction measurements

X-ray diffraction (XRD) and grazing incidence XRD (GIXRD) measurements before and after the irradiation were performed. The GIXRD measurements were performed at an incidence angle of $a_0 = 1.1°$ in order to maximize the diffracted intensity. The measurements were carried out at room temperature using the Bruker D8 Discover diffractometer with a line focus Cu-K_α X-ray

source and a parallel beam stemming from a Göbbel mirror. The lattice constant, a, of the films was determined by the position of the Bragg peaks after correction for the shift caused by refraction [26]. The volume – averaged mean grain size was determined from the XRD spectra using the Scherrer equation [27],[28]

$$\langle D \rangle_V = \frac{0.9 K_s \lambda}{FWHM_{2\theta_B} \cos\theta_B} \quad (2)$$

where λ is the wavelength of the incident X-rays, θ_B is the Bragg angle of the XRD peak centroid, $FWHM_{2\theta_B}$ is the corresponding Full-Width at Half-Maximum (FWHM) of the (110) peak in radians after the subtraction of the instrumental broadening [28], [29] and K_s is the Scherrer constant which is related to the actual shape of the crystallite and takes numerical values around unity [30]. The instrumental broadening was determined by the measured FWHM of the (400) Bragg peak of a Si(100) single crystal. In the above described procedure it is assumed that the Bragg peak broadening is due to grain size and any strain effects contributing to the broadening are neglected. This is a quite good approximation since the Lorentzian part of the Bragg peak line profile is more than about 70% indicating that the grain size effects dominate Bragg peak broadening.

2.5. X-ray reflectivity

The layered structure of the films before and after irradiation was investigated using X-ray Reflectivity (XRR) using the D8 Discover Bruker diffractometer in reflectivity mode with exit and receiving slits of 0.1 mm and an antiscatter slit of 0.2 mm. XRR spectra were fitted using GenX software [31], [32] in order to determine the film structure (thickness, density, roughness).

2.6. Neutron reflectivity

The magnetization as a function of depth was determined employing Polarised Neutron Reflectivity (PNR) [33] measurements at POLREF facility, at ISIS neutron spallation source, at Rutherford-Appleton Laboratory (RAL) in United Kingdom. The measurements took place at room temperature at an applied in plane field of 1.085 T in order to create a saturated long range order in the FeCr film [18]. POLREF uses a broad band neutron time-of-flight (TOF) method for determining the wavelength, and hence the magnitude of momentum transfer $\mathbf{Q} = \mathbf{k}' - \mathbf{k}$, where $\mathbf{k}'$ and $\mathbf{k}$ are the wave vectors of the scattered and incident beam respectively, at fixed angles, θ, of the detector. The detector angle was set to 0.6^o and the Q range varied from 0.093 to 0.65 nm^{-1}. In PNR measurements neutrons are incident with their spin or their magnetic moment either parallel (+) or antiparallel (−) to the applied field. The neutron reflectivity R^+ corresponding to the spin of incident neutron beam parallel to the applied magnetic field (spin up) and the reflectivity R^- corresponding to the spin being antiparallel to the applied filed (spin

down) are measured. The PNR data were least squares fitted using the GenX software [31],[32]. A short description of the use of the PNR technique for the determination of the magnetization is provided in [18].

3. Results

3.1. Structural changes due to Fe+ irradiations

The structural characterization of the irradiated films were determined employing XRR and XRD techniques. Regarding the FeCr layer, the thickness was found to vary between 69 and 72 nm, the mass density remained practically the same after irradiation, varying between (7.48±0.04) g·cm^{-3} for the unirradiated sample and (7.58±0.06) g·cm^{-3} after irradiation at 20 dpa. The roughness was of the order of 2-3 nm.

The as fabricated and irradiated films crystallize in the bcc structure of the $Im\bar{3}m$ space group. The lattice constant of the films versus the dose, d, in dpa is presented in **Figure 2**. It is observed that after the exposure of the unirradiated film at 300 °C and a damage of 0.5 dpa (second point in **Figure 2**), the lattice constant is reduced sharply from its unirradiated value (first point **Figure 2**). Additional damage increases the lattice constant from that of the 0.5 dpa. It should be remembered that each point in **Figure 2** corresponds to a different sample. There are two possible explanations about this sequence of lattice constant change versus irradiation dose. Either, as the sample is initially irradiated to 0.5 dpa its lattice constant is reduced and additional irradiation results in lattice constant increase. The second explanation would be that as the sample temperature is raised from room temperature to 300 °C the lattice constant decreases (for example crystallinity enhancement), whereas the irradiation effect would be the subsequent lattice constant increase. The second conjecture seems more plausible and, thus, we assume that there is an initial, due to sudden temperature increase, lattice constant decrease and that the lattice constant at the first irradiation dose (0.5 dpa) reflects the equilibrium lattice constant at 300 °C. Under this assumption the dependence of the lattice constant versus dose in **Figure 2** for $d \geq 0.5$ dpa can be described by the equation

$$a = a_0 + a_{inc}\left(1 - exp\left(-\frac{d}{d_a}\right)\right) \quad (3)$$

where the least squares determined values are: $a_0 = (2.859 \pm 0.001)$ Å, $a_{inc} = (0.003 \pm 0.001)$ Å and $d_a = (2.0 \pm 1.0)$ dpa^{-1}. The asymptotic value of lattice constant is $\lim_{d\to\infty} a = a_0 + a_{inc} = (2.862 \pm 0.002)$ Å.

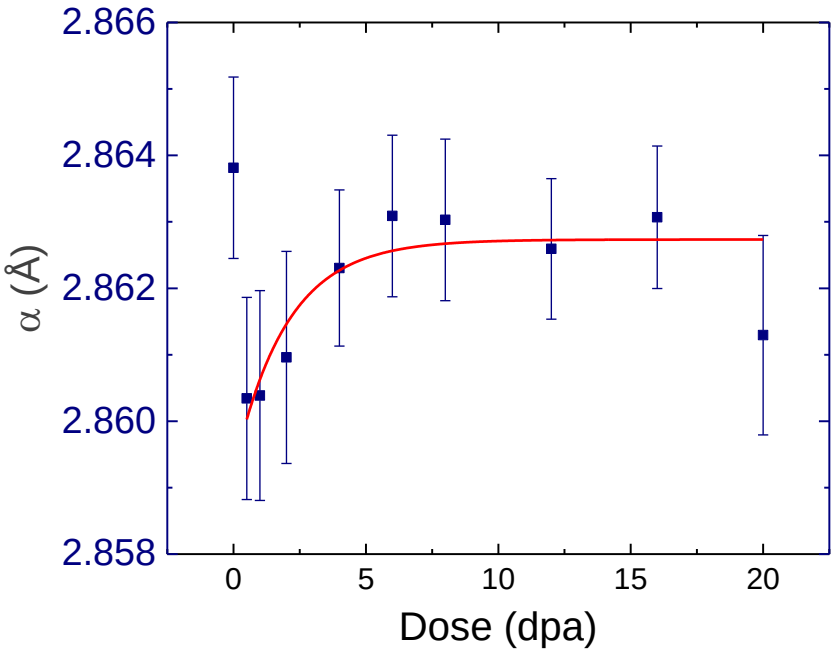

Figure 2: Lattice constant determined from GIXRD measurements. The solid line is the least square fit of Eq. (3) to the data.

The averaged mean grain size determined using Eq. (2) is presented in **Figure 3** as a function of irradiation dose, d, in dpa. It is observed that the grain size increases monotonically with dose. There is an initial stage where the grain size increases abruptly and a second stage where it remains almost constant. The variation of the grain size versus dose, d, in dpa can be described by the equation

$$D(d) = D_0 + D_{incr}\left(1 - exp\left(-\frac{d}{d_g}\right)\right) \qquad (4)$$

where the least squares constants are: $D_0 = (21 \pm 2)$ nm, $D_{incr} = (13 \pm 2)$ nm and $d_g = (1.1 \pm 0.4)$ dpa.

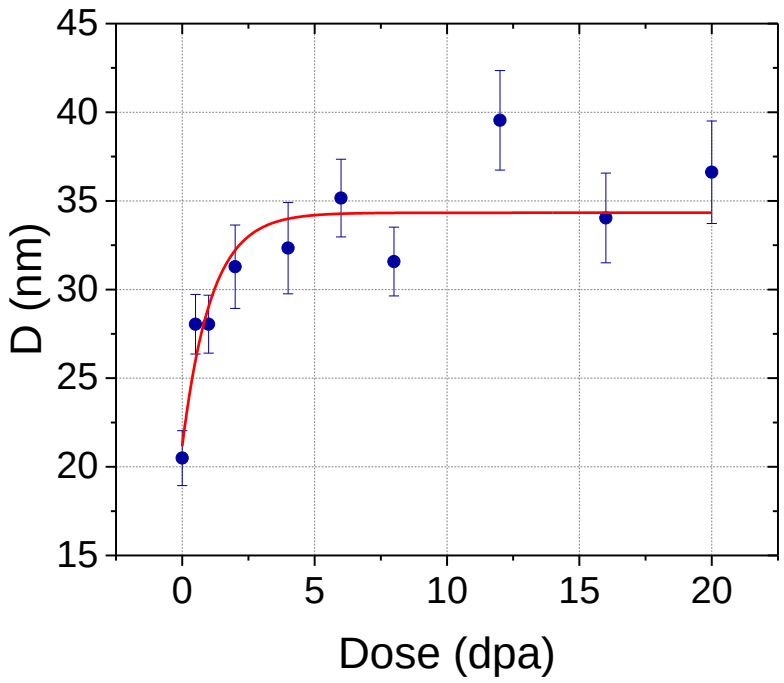

Figure 3: Averaged mean grain size as a function of irradiation dose. The solid line is a least-square fit of Eq. (4) to the data.

3.2. Determination of the Cr content versus damage.

In **Figure 4**(a) the R^+ and R^- reflectivities for the unirradiated sample and that irradiated at the dose of 4 dpa at 300 ^{o}C are presented with the least squares fitted curves to the data. In **Figure 4**(b) the spin asymmetry $R^+ - R^-$ multiplied by Q^4, in order to remove the asymptotic behavior of the reflectivity, is presented as a function of Q. The spin asymmetry is connected with the magnetization of the film and the observed spin asymmetry increase versus irradiation dose corresponds to magnetization increase.

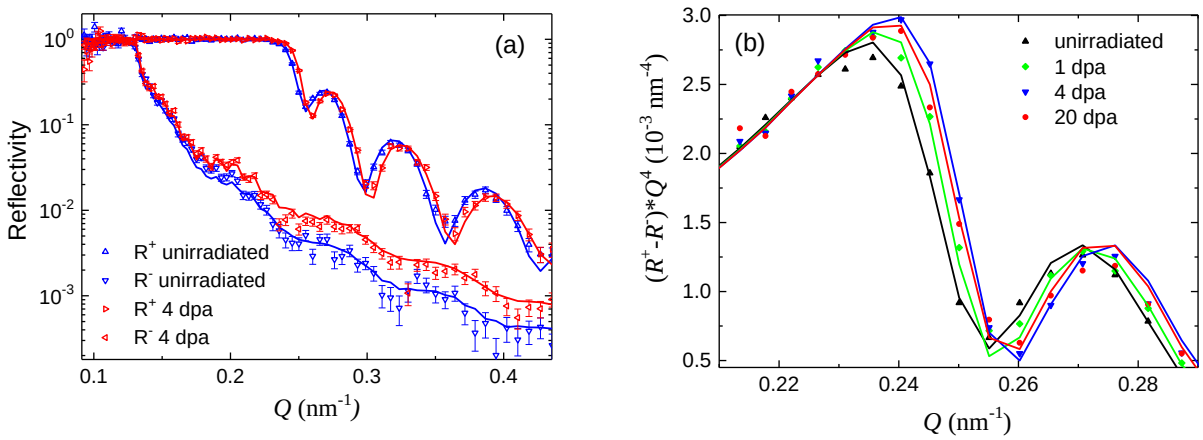

Figure 4: PNR spectra for the Fe-10%atCr films. The solid lines are least squares fits to the experimental data. (a) Spin up, R^+, and spin down, R^-, reflectivity versus scattering length, Q, for the unirradiated and the 4 dpa irradiated sample. (b) Spin asymmetry, $(R^+ - R^-)\cdot Q^4$, at the critical edge, for the unirradiated and the 1, 4 and 20 dpa irradiated samples.

From the least squares fit to the PNR data the layered structure (thickness, density, roughness) and magnetization of the films was determined. The layered structure from PNR analysis is in good agreement with the one obtained from XRR analysis with minor deviations in the atomic density of the layers and the interface roughness. These differences have their origin in the nature of the interaction that takes place in each case (nuclear and electromagnetic interactions, respectively) which results in different penetration depths for X-Rays and neutrons and different contrast/resolution for the elements for each particle. It should be also noted that the scattering length of Cr and Fe are very different for neutrons contrary to the corresponding scattering factors for X-rays which are very close. Thus, neutron reflectivity is sensitive to Cr structures (e.g. Cr_2O_3 top layer). The determined magnetization of the Fe-Cr layer increases as the dose increases up to about 4 dpa and does not change, within error bars, for further increase of the dose.

The Cr solute concentration in the matrix after an irradiation can be determined by the magnetization of Fe-Cr alloys (with Cr concentration in the range 0-15 at%) both in bulk and film form measured by PNR and magnetization measurements and the equation [18]

$$x_{Cr}(at\%) = A\left(at\% \Big/ \mu_B/at\right)(m_0 - m) \qquad (4)$$

where, x_{Cr} is the Cr concentration in at%, m is the average magnetic moment determined by the analysis of the PNR spectra and magnetization measurements using a Vibrating Sample Magnetometer. The constants A and m_0 have been determined experimentally as described in

[18]. $m_0 = (2.12 \pm 0.01)\,\mu_B$ / a t coincides with the magnetic moment of pure Fe at room temperature. $A = (41.0 \pm 1.4)$ (at%/μ_B/at) reflects the variation of the magnetization of Fe-Cr alloys versus Cr content for Cr concentrations up to 15 at%.

The solute Cr concentration in the Fe-Cr matrix of the samples irradiated at 300 ^{o}C, is presented as a function of irradiation dose, d, in **Figure 5**. Also previous results for Fe-10at%Cr alloys Fe+ irradiated at room temperature [18] are plotted for comparison. The solid lines are the least squares fittings of the data using the equation

$$C(d) = C_0 - C_\infty (1 - e^{-d/d_0}) \quad (5)$$

where C_0 is the initial solute Cr content, $C_{eq} = C_0 - C_\infty$ is the equilibrium solute concentration of Cr and d_0 the radiation damage saturation constant. The fitted values of the parameters of Eq. (5) are presented in **Table 1**. The initial Cr solute concentration, C_0, in the Fe-Cr layer determined from PNR analysis is in good agreement, within errors, with that resulted from X-ray fluorescence spectroscopy ((9.6 ± 1.0) at%) and Rutherford backscattering spectroscopy ((11 ± 1) at%) measurements ([34], [35]). From **Figure 5** it is concluded that equilibrium conditions are reached at about 4 dpa for irradiations at 300 °C and at about 6 dpa in the case of room temperature irradiations.

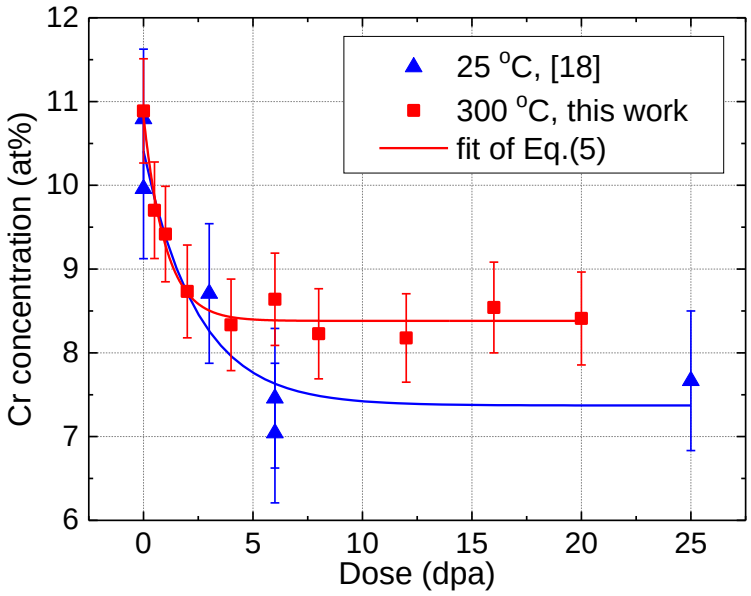

Figure 5: Solute Cr concentration in the Fe-Cr matrix as a function of dose for Fe-10at%Cr irradiated at 300 ^{o}C (this work) and at 25 °C [18] at the dose rate of 0.002 dpa/s. The solid lines are the least squares fit of Eq. (5) to the experimental data.

Table 1: Fitted values for the parameters in Eq. (5) to the experimental data in **Figure 5**.

T_{irr} (°C)	C_0 (at%)	C_∞ (at%)	C_{eq} (at%)	d_0 (dpa)
25 [18]	10.6 ± 0.4	3.4 ± 0.3	7.2 ± 0.5	2.2 ± 0.7
300 (this work)	10.8 ± 0.2	2.4 ± 0.2	8.4 ± 0.3	1.00 ± 0.18

4. Discussion

Irradiation of Fe-10at%Cr films of 70 nm thick with 490 keV Fe+ ions at 300 °C results in: a) lattice constant increase, b) grain size increase and c) Cr depletion in the matrix. These changes occur largely up to 4 dpa and afterwards little change is observed. The dependence of all three properties versus dpa dose, d , is described by an equation of the form

$$p(d) \sim p_\infty \left(1 - \exp(-\frac{d}{d_p})\right) \quad (6)$$

where the activation constant, d_p , for the different parameters varies between (1.00±0.18) dpa and (2.0±1.0) dpa.

The central finding of this work is that Fe+ ion irradiation at 300 °C results in the removal of Cr from the matrix. This removal initially, up a dose of 4 dpa, is dose dependent, and afterwards it appears that the system is under a dynamic equilibrium. The same conclusion has been drawn also for Fe+ ion irradiation of Fe-10at%Cr at 25 °C. Comprehension of this dynamic equilibrium, common in both irradiation temperatures, is important for a deeper understanding of the irradiation effects in FeCr. For the Fe-Cr alloys, the Cr content of 10 at.% lies within the solvus area [36], [37] and the phase boundary of their miscibility gap is placed between 500 and 510 °C [38], [39]. For the irradiation temperature of 300 °C, or even more at 25 °C, thermal diffusion is not sufficient to drive the decomposition of the alloy into Fe – rich (α) and Cr – rich (α′) phases. Therefore, any variation in solute Cr concentration in the material matrix can mainly be attributed to irradiation induced diffusion.

The effects observed are seemingly a result of both irradiation and temperature annealing. However, from **Figure 5** it can be inferred that the effect of temperature annealing is much less crucial than that of the irradiation. The system has reached an apparent equilibrium after a dose of about 4 dpa and temperature annealing of about 30 mins. Notwithstanding that the temperature annealing continues for more than additional two hours no effects are observed. Furthermore, the irradiation studies need to reflect both the temperature and irradiation effects, i.e. the real irradiation conditions of a material application.

Under the above premises a visualization of the Fe+ ion irradiation on the Cr content of the FeCr matrix will be attempted. Initially the Cr concentration of about 10 at% is above the solubility

limit at these temperatures (25 and 300 °C) or the free energy of the system is not at its minimum, as indicated by the phase diagram. However, the kinetics (diffusion) at these temperatures is extremely slow so the system cannot be driven to its minimum free energy. The Fe+ ion irradiation generates vacancies and Cr interstitials. Substitutional Cr migrates via the vacancies and together, to a much lesser degree, with the generated Cr interstitials accumulate to different sinks. Such sinks may be grain boundaries, dislocations, vacancy clusters etc. This matrix Cr depletion and Cr clustering/segregation versus vacancy (dpa) generation lowers the free energy of the system. After 4 dpa at 300 °C or 6 dpa at 25 °C the free energy of the system is close to minimum and the Cr content in the matrix remains almost constant. Corroboration to this rational is that the alloy Fe-5at%Cr even after 50 dpa Fe+ irradiation remains unchanged [18], i.e. it is at its minimum free energy which the Fe-10at%Cr alloy attains after irradiation of around 4 or 6 dpa for 300 and 25 °C, respectively.

At a specific Cr concentration, depending on the temperature (C_{eq} in **Table 1**), a dynamic equilibrium is established in the matrix. The constituents of this equilibrium are the Cr concentration in the matrix and at the different sinks and the Frenkel pair generation by 490 keV Fe+ ion irradiation. In this dynamic equilibrium Cr atoms move from the matrix to the sinks and vice versa with the Cr content in the matrix remaining constant. It might be hypothesized that larger Cr agglomerates grow at the expense of smaller ones (Ostwald ripening) [40] as this will further lower the free energy of the system. The Cr concentration of this dynamic equilibrium is close to that expected from the phase diagram [37]. It is necessary the effect of the rate of defect production to be assessed. This is important for extending these findings to neutron irradiations in a fusion plant where a much lower rate of PKA production is foreseen. An investigation for determining the effect of the rate of damage (in this work it has been 0.002 dpa/s) is under way.

From the above discussion it is concluded that during Fe+ irradiation Cr moves from the matrix to sinks. Experiments that have been performed so far give different and sometimes contrary results depending on the particle used to irradiate Fe–Cr alloys. At similar irradiation conditions dislocation loops have been found homogenously distributed after Fe-ion irradiation [12] and these could be possible sites for Cr segregation. The formation of Cr – rich α′ precipitates with >85 at% Cr concentration have been only observed under neutron irradiations at around 300 °C in model Fe-Cr alloys with 9 at% Cr or more [12], [41], [42], [43], [44], [45], [46], [47], [48], [49] but not under self – ion irradiation at similar irradiation conditions, where only limited radiation-driven clustering has been observed [50], [51], [52], [53]. This is attributed to the higher dose rates by orders of magnitude that are present in the case of neutrons [12], [50], [51], [52], [53] and to the high concentration of injected interstitials [54], [51]. The agglomeration of Cr around the grain boundaries is energetically more favorable as the surface energy and thus the free energy is reduced. Under Fe+ irradiation probably are not formed extensive vacancy clusters to assist heterogeneous nucleation of Cr. However, during neutron irradiation such clusters might be formed or clusters from transmutation elements which act as nucleation sites for α′ precipitation [44].

The lattice constant and grain size depend on dpa in a similar manner as the depletion of the Cr from the matrix i.e. after the initial increase at low doses both remain almost constant for doses higher than 4 dpa. The as fabricated Fe-Cr film with respect to the average grain size is not at its minimum free energy [55], [56] as increase of the grain size will result in the reduction of the surface energy. Ion irradiation has been observed to induce grain growth in thin polycrystalline metal film and it has been experimentally and theoretically investigated in a number of studies such as [57], [58], [16]. Fe+ irradiation-induced grain growth is subject to the same driving force as thermal grain growth, but the atomic transport mechanisms arises either from thermal spikes or migrating vacancies and interstitials [59]. At the steady state (d >4 dpa) the number of grains has been reduced to one third whereas the total grain surface has been reduced to 70% compared to the unirradiated sample.

The lattice constant of the unirradiated sample, corresponding to Cr concentration of 10 at%, is (2.864±0.001) Å and that at the high damage (see **Figure 2** and text), corresponding to Cr concentration of 8.4 at% is (2.862±0.001) Å. This is in correspondence with the general tendency of Fe-Cr alloys in which reduction of the Cr content results in the decrease of the lattice constant [60]. The dependence of lattice constant versus damage has similar behavior as that observed for the Cr content and grain size i.e. it attains an equilibrium value as described by Eq. (5). The increase of the lattice constant versus dose it has to be attributed to strain relaxation effects i.e. the lattice after a dose above 4 dpa attains a strain free state.

5. Conclusions

Fe-10at%Cr alloys in the form of thin films were irradiated at 300 °C with 490 keV Fe^+ ions with a damage rate of 0.002 dpa/s and at doses ranging from 0.5 to 20 dpa. The irradiation results in a dose dependent alteration of the lattice constant, grain size and Cr content in the matrix. For doses up to 4 dpa there is an increase of the lattice constant and grain size and a decrease of the Cr solute concentration in the matrix. For doses above 4 dpa the system is in a dynamic equilibrium and these three parameters remain almost constant. This indicates that the system above 4 dpa is at its minimum free energy and the continuous generation of defects by the Fe+ ions does not produce any effects. Similar effects had been observed at the Fe+ ion irradiations performed on Fe-10at%Cr at ambient temperature [18]. The equilibrium concentrations of Cr in the matrix at 300 °C and room temperature [26] correspond to those expected from the phase diagram of Fe-Cr alloys [37]. The experimental techniques employed determined accurately an important parameter, the Cr solute concentration in the matrix versus irradiation dose. To where the solute Cr removed from the matrix accumulates and in what form need further investigation. The Cr probably segregates at grain boundaries as it has been observed in ferritic-martensitic alloys [61],[62] or at dislocation loops as found in electron irradiated Fe-10at% [63]. As the kinetics of Cr depletion and α′ formation depend on the number of sinks [64] and this number is

connected by the damaging rate an investigation on examining the effect of the dose rate (dpa/s) on the kinetics and equilibrium values is under way. This is important for extending these findings to neutron irradiations in a fusion plant where it will be lower rate of PKA production.

.

Acknowledgments

This work has been carried out within the framework of the EUROfusion Consortium and has received funding from the Euratom research and training programme 2014-2018 and 2019-2020 under Grant Agreements No. 633053. The views and opinions expressed herein do not necessarily reflect those of the European Commission. Experiments at the ISIS Neutron and Muon Source were supported by a beamtime allocation from the Science and Technology Facilities Council. The use of the Ion Beam Center facilities at Helmholtz-Zentrum Dresden-Rossendorf is acknowledged. Also, the funding from the Hellenic General Secretariat for Research and Innovation for the Greek National Programme for the Controlled Thermonuclear Fusion is acknowledged.

References

[1] R. Lässer *et al.*, "Structural materials for DEMO: The EU development, strategy, testing and modelling," *Fusion Eng. Des.*, vol. 82, no. 5–14, pp. 511–520, 2007, doi: 10.1016/j.fusengdes.2007.06.031.

[2] S. J. Zinkle, "Advanced materials for fusion technology," *Fusion Eng. Des.*, vol. 74, no. 1–4, pp. 31–40, 2005, doi: 10.1016/j.fusengdes.2005.08.008.

[3] D. Stork *et al.*, "Materials R&D for a timely DEMO: Key findings and recommendations of the EU Roadmap Materials Assessment Group," *Fusion Eng. Des.*, vol. 89, no. 7–8, pp. 1586–1594, 2014, doi: 10.1016/j.fusengdes.2013.11.007.

[4] S. I. Porollo, A. M. Dvoriashin, A. N. Vorobyev, and Y. V. Konobeev, "The microstructure and tensile properties of Fe-Cr alloys after neutron irradiation at 400°C to 5.5-7.1 dpa," *J. Nucl. Mater.*, vol. 256, no. 2–3, pp. 247–253, 1998, doi: 10.1016/S0022-3115(98)00043-9.

[5] F. Garner, M. Toloczko, and B. Sencer, "Comparison of swelling and irradiation creep behavior of fcc-austenitic and bcc-ferritic/martensitic alloys at high neutron exposure," *J. Nucl. Mater.*, vol. 276, no. 1–3, pp. 123–142, 2000, doi: 10.1016/S0022-3115(99)00225-1.

[6] E. A. Little and D. A. Stow, "Void-swelling in irons and ferritic steels: II. An experimental survey of materials irradiated in a fast reactor," *J. Nucl. Mater.*, vol. 87, no. 1, pp. 25–39, 1979, doi: 10.1016/0022-3115(79)90123-5.

[7] M. B. Toloczko, F. A. Garner, and C. R. Eiholzer, "Irradiation creep and swelling of the US fusion heats of HT9 and 9Cr-1Mo to 208 dpa at ~ 400°C," *J. Nucl. Mater.*, vol. 212–215, no. PART 1, pp. 604–607, 1994, doi: 10.1016/0022-3115(94)90131-7.

[8] R. L. Klueh and A. T. Nelson, "Ferritic/martensitic steels for next-generation reactors," *J. Nucl. Mater.*, vol. 371, no. 1–3, pp. 37–52, 2007, doi: 10.1016/J.JNUCMAT.2007.05.005.

[9] R. L. Klueh, K. Ehrlich, and F. Abe, "Ferritic/martensitic steels: promises and problems," *J. Nucl. Mater.*, vol. 191–194, no. 1992, pp. 116–124, 1992, doi: 10.1016/S0022-3115(09)80018-4.

[10] Y. Katoh and D. S. Gelles, "Swelling and dislocation evolution in simple ferritic alloys irradiated to high fluence in FFTF/MOTA ", *J. Nucl. Mater.*, vol. 225, pp. 154–162, 1995, https://doi.org/10.1016/0022-3115(94)00669-5.

[11] C. D. Hardie, G. R. Odette, Y. Wu, S. Akhmadaliev, and S. G. Roberts, "Mechanical properties and plasticity size effect of Fe-6%Cr irradiated by Fe ions and by neutrons," *J. Nucl. Mater.*, vol. 482, pp. 236–247, 2016, doi: 10.1016/j.jnucmat.2016.10.028.

[12] M. Hernández-Mayoral, C. Heintze, and E. Oñorbe, "Transmission electron microscopy investigation of the microstructure of Fe-Cr alloys induced by neutron and ion irradiation at 300°C," *J. Nucl. Mater.*, vol. 474, pp. 88–98, 2016, doi: 10.1016/j.jnucmat.2016.03.002.

[13] Shuoxue Jin, Bing Mo, Weiping Zhang, Tongmin Zhang, Yang Li, Liping Guo, Xingzhong Cao, Baoyi Wang, "Towards understanding the evolution of dislocation loops and their interaction with vacancies in Fe9Cr alloy during the irradiation swelling incubation period," *Materialia*, vol. 5, p. 100241, 2019, doi: 10.1016/j.mtla.2019.100241.

[14] J. B. J. Chapman, P. W. Ma, and S. L. Dudarev, "Dynamics of magnetism in Fe-Cr alloys with Cr clustering," *Phys. Rev. B*, vol. 99, no. 18, p. 184413, 2019, doi: 10.1103/PhysRevB.99.184413.

[15] P. Derlet and S. Dudarev, "Million-atom molecular dynamics simulations of magnetic iron," *Prog. Mater. Sci.*, vol. 52, no. 2–3, pp. 299–318, 2007, doi:

10.1016/j.pmatsci.2006.10.011.
[16] K. Papamihail, K. Mergia, F. Ott, Yves Serruys, Th. Speliotis, G. Apostolopoulos, S. Messoloras, "Fe^{+}ion irradiation induced changes in structural and magnetic properties of iron films," *Nucl. Mater. Energy*, vol. 9, 459-464, 2016, doi: 10.1016/j.nme.2016.03.006.
[17] K. Papamihail, K. Mergia, F. Ott, Yves Serruys, Th. Speliotis, G. Apostolopoulos, and S. Messoloras, "Magnetic effects induced by self-ion irradiation of Fe films," *Phys. Rev. B*, vol. 93, no. 10, 100404(R), 2016, doi: 10.1103/PhysRevB.93.100404.
[18] K. Mergia, E. O. Tsompopoulou, S. Dellis, C. H. Marrows, I. Michelakaki, C. Kinane, A. Caruana, S. Langridge, A. P. Douvalis, C. Cabet and S Messoloras, "Phase stability of Fe-5at%Cr and Fe-10at%Cr films under Fe+ ion irradiation," *J. Phys. Condens. Matter*, vol. 32, no. 18, 2020, doi: 10.1088/1361-648X/ab69a1.
[19] M. R. Gilbert, T. Eade, C. Bachmann, U. Fischer, and N. P. Taylor, "Activation, decay heat, and waste classification studies of the European DEMO concept," *Nucl. Fusion*, vol. 57, 046015 (14pp), 2017, https://doi.org/10.1088/1741-4326/aa5bd7
[20] R. S. Nelson, "The use of ion beams to study radiation effects in metals", Contemporary Physics, vol. 19, no.6, 543-569, 1978, https://doi.org/10.1080/00107517808207700.
[21] M. R. Gilbert and J. C. Sublet, "Differential dpa calculations with SPECTRA-PKA," *J. Nucl. Mater.*, vol. 504, pp. 101–108, 2018, doi: 10.1016/j.jnucmat.2018.03.032.
[22] G. Federici, W. Biel, M. R. Gilbert, R. Kemp, N. Taylor, and R. Wenninger, "European DEMO design strategy and consequences for materials," *Nucl. Fusion*, vol. 57, no. 9, p. 092002, 2017, doi: 10.1088/1741-4326/57/9/092002.
[23] J. F. Ziegler, J. P. Biersack U. and Littmark, The Stopping and Range of Ions in Solids, New York: Pergamon, 1985.
[24] "ASTM International - ASTM E693-12E1 - Standard Practice for Characterizing Neutron Exposures in Iron and Low Alloy Steels in Terms of Displacements Per Atom (DPA)".
[25] S. Agarwal, Y. Lin, C. Li, R. E. Stoller, and S. J. Zinkle, "On the use of SRIM for calculating vacancy production: Quick calculation and full-cascade options," *Nucl. Instruments Methods Phys. Res. Sect. B Beam Interact. with Mater. Atoms*, vol. 503, pp. 11–29, 2021, doi: 10.1016/j.nimb.2021.06.018.
[26] S. Wroński, K. Wierzbanowski, a. Baczmański, a. Lodini, C. Braham, and W. Seiler, "X-ray grazing incidence technique—corrections in residual stress measurement—a review," *Powder Diffr.*, vol. 24, no. S1, pp. S11–S15, 2012, doi: 10.1154/1.3139054.
[27] P. Scherrer, "Bestimmung der Größe und der inneren Struktur von Kolloidteilchen mittels Röntgenstrahlen," *Nachrichten von der Gesellschaft der Wissenschaften zu Göttingen, Math. Klasse*, vol. 1918, pp. 98–100.
[28] M. Birkholz, *Thin Film Analysis by X-Ray Scattering*, Wiley-VCH Verlag GmbH & Co, 2006.
[29] A. R. Stokes, "A Numerical Fourier-analysis Method for the Correction of Widths and Shapes of Lines on X-ray Powder Photographs," *Proc. Phys. Soc.*, vol. 61, no. 4, p. 382, 1948, doi: 10.1088/0959-5309/61/4/311.
[30] J. I. Langford, D. Louër, and IUCr, "Diffraction line profiles and Scherrer constants for materials with cylindrical crystallites," *urn:issn:0021-8898*, vol. 15, no. 1, pp. 20–26, 1982, doi: 10.1107/S0021889882011297.
[31] M. Björck and G. Andersson, "GenX: An extensible X-ray reflectivity refinement program utilizing differential evolution," *J. Appl. Crystallogr.*, vol. 40, no. 6, pp. 1174–1178, 2007, doi: 10.1107/S0021889807045086.

[32] https://aglavic.github.io/genx/.
[33] J. F. Ankner and G. P. Felcher, "Polarized-neutron reflectometry," *J. Magn. Magn. Mater.*, vol. 200, no. 1–3, pp. 741–754, 1999, doi: 10.1016/S0304-8853(99)00392-3.
[34] E. Tsompopoulou, and K. Mergia, "Energy Dispersive X-Ray Fluorescence Spectroscopy and Applications in Material Science", *HNPS Advances in Nuclear Physics*, vol. 21, pp. 145–147, 2019, http://dx.doi.org/10.12681/hnps.2020.
[35] P. Jussieu, "Rutherford backscattering spectrometry," Vacuum, vol. 37, pp. 429–432, 1987, https://doi.org/10.1016/0042-207X(87)90327-7.
[36] W. Xiong, M. Selleby, Q. Chen, J. Odqvist, and Y. Du, "Phase equilibria and thermodynamic properties in the Fe-Cr system," *Crit. Rev. Solid State Mater. Sci.*, vol. 35, no. 2, pp. 125–152, 2010, doi: 10.1080/10408431003788472.
[37] G. Bonny, D. Terentyev, and L. Malerba, "On the α-α′ miscibility gap of Fe-Cr alloys," *Scr. Mater.*, vol. 59, no. 11, pp. 1193–1196, 2008, doi: 10.1016/j.scriptamat.2008.08.008.
[38] S. M. Dubiel and G. Inden, "On the miscibility gap in the Fe-Cr system: a Moessbauer study on long term annealed alloys," *Zeitschrift fuer Met. Res. Adv. Tech.*, vol. 78, no. 8, pp. 544–549, 1987, https://doi.org/10.1515/ijmr-1987-780802.
[39] S. Novy, P. Pareige, and C. Pareige, "Atomic scale analysis and phase separation understanding in a thermally aged Fe–20 at.%Cr alloy," *J. Nucl. Mater.*, vol. 384, no. 2, pp. 96–102, 2009, doi: 10.1016/J.JNUCMAT.2008.10.008.
[40] I. M. Lifshitz and V. V. Slyozov, "The kinetics of precipitation from supersaturated solid solutions," *J. Phys. Chem. Solids*, vol. 19, no. 1–2, pp. 35–50, 1961, doi: 10.1016/0022-3697(61)90054-3.
[41] M. Bachhav, G. Robert Odette, and E. A. Marquis, "α′ precipitation in neutron-irradiated Fe-Cr alloys," *Scr. Mater.*, vol. 74, pp. 48–51, 2014, doi: 10.1016/j.scriptamat.2013.10.001.
[42] V. Kuksenko, C. Pareige, and P. Pareige, "Cr precipitation in neutron irradiated industrial purity Fe-Cr model alloys," *J. Nucl. Mater.*, vol. 432, no. 1–3, pp. 160–165, 2013, doi: 10.1016/j.jnucmat.2012.07.021.
[43] V. Kuksenko, C. Pareige, and P. Pareige, "Intra granular precipitation and grain boundary segregation under neutron irradiation in a low purity Fe-Cr based alloy," *J. Nucl. Mater.*, vol. 425, no. 1–3, pp. 125–129, 2012, doi: 10.1016/j.jnucmat.2011.10.031.
[44] E. R. Reese, M. Bachhav, P. Wells, T. Yamamoto, G. Robert Odette, and E. A. Marquis, "On α′ precipitate composition in thermally annealed and neutron-irradiated Fe- 9-18Cr alloys," *J. Nucl. Mater.*, vol. 500, pp. 192–198, 2018, doi: 10.1016/j.jnucmat.2017.12.036.
[45] F. Bergner, C. Pareige, V. Kuksenko, L. Malerba, P. Pareige, A. Ulbricht, A. Wagner, "Critical assessment of Cr-rich precipitates in neutron-irradiated Fe-12 at%Cr: Comparison of SANS and APT," *J. Nucl. Mater.*, vol. 442, no. 1–3, pp. 463–469, 2013, doi: 10.1016/j.jnucmat.2013.05.023.
[46] M. Lambrecht and L. Malerba, "Positron annihilation spectroscopy on binary Fe-Cr alloys and ferritic/martensitic steels after neutron irradiation," *Acta Mater.*, vol. 59, no. 17, pp. 6547–6555, 2011, doi: 10.1016/j.actamat.2011.06.046.
[47] M. H. Mathon, Y. De Carlan, G. Geoffroy, X. Averty, A. Alamo, and C. H. De Novion, "A SANS investigation of the irradiation-enhanced α-α′ phases separation in 7-12 Cr martensitic steels," *J. Nucl. Mater.*, vol. 312, no. 2–3, pp. 236–248, 2003, doi: 10.1016/S0022-3115(02)01630-6.
[48] W. Y. Chen, Y. Miao, J. Gan, M. A. Okuniewski, S. A. Maloy, and J. F. Stubbins,

"Neutron irradiation effects in Fe and Fe-Cr at 300 °c," *Acta Mater.*, vol. 111, pp. 407–416, 2016, doi: 10.1016/j.actamat.2016.03.060.
[49] W. Y. Chen, Yinbin Miao, Yaqiao Wub, Carolyn A. Tomchik, Kun Mo, Jian Gan, Maria A. Okuniewski, Stuart A. Maloy, James F. Stubbins, "Atom probe study of irradiation-enhanced α precipitation in neutron-irradiated Fe-Cr model alloys," *J. Nucl. Mater.*, vol. 462, pp. 242–249, 2015, doi: 10.1016/j.jnucmat.2015.04.005.
[50] C. Pareige, V. Kuksenko, and P. Pareige, "Behaviour of P, Si, Ni impurities and Cr in self ion irradiated Fe-Cr alloys - Comparison to neutron irradiation," *J. Nucl. Mater.*, vol. 456, pp. 471–476, 2015, doi: 10.1016/j.jnucmat.2014.10.024.
[51] E. R. Reese, N. Almirall, T. Yamamoto, S. Tumey, G. Robert Odette, and E. A. Marquis, "Dose rate dependence of Cr precipitation in an ion-irradiated Fe 18Cr alloy," *Scr. Mater.*, vol. 146, pp. 213–217, 2018, doi: 10.1016/j.scriptamat.2017.11.040.
[52] E. Marquis, B. Wirth, and G. Was, "Characterization and Modeling of Grain Boundary Chemistry Evolution in Ferritic Steels under Irradiation", United States: N. p., 2016. Web. doi:10.2172/1248953.
[53] C. D. Hardie, C. A. Williams, S. Xu, and S. G. Roberts, "Effects of irradiation temperature and dose rate on the mechanical properties of self-ion implanted Fe and Fe-Cr alloys," *J. Nucl. Mater.*, vol. 439, no. 1–3, pp. 33–40, 2013, doi: 10.1016/j.jnucmat.2013.03.052.
[54] O. Tissot, C. Pareige, E. Meslin, B. Décamps, and J. Henry, "Influence of injected interstitials on α′ precipitation in Fe–Cr alloys under self-ion irradiation," *Mater. Res. Lett.*, vol. 5, no. 2, pp. 117–123, 2017, doi: 10.1080/21663831.2016.1230896.
[55] N. Zhou and J. Luo, "Developing thermodynamic stability diagrams for equilibrium-grain-size binary alloys," *Mater. Lett.*, vol. 115, pp. 268–271, 2014, doi: 10.1016/j.matlet.2013.09.093.
[56] M. Saber, C. C. Koch, and R. O. Scattergood, "Thermodynamic grain size stabilization models: An overview," *Mater. Res. Lett.*, vol. 3, no. 2, pp. 65–75, 2015, doi: 10.1080/21663831.2014.997894.
[57] D. Kaoumi, A. T. Motta, and R. C. Birtcher, "Grain Growth in Nanocrystalline Metal Thin Films under In Situ Ion-Beam Irradiation," *Journal of ASTM International*, vol. 4, no. 8, pp. 1–13, 2007.
[58] D. E. Alexander and G. S. Was, "Thermal-spike treatment of ion-induced grain growth: Theory and experimental comparison", *Phys. Rev. B*, vol. 47, no. 6, 1993.
[59] D. Kaoumi, a. T. Motta, and R. C. Birtcher, "A thermal spike model of grain growth under irradiation," *J. Appl. Phys.*, vol. 104, no. 7, p. 073525, 2008, doi: 10.1063/1.2988142.
[60] G. D. Preston, "The London, Edinburgh, and Dublin Philosophical Magazine and Journal of Science Series 7 XXXV. An X-ray examination of Iron-Chromium alloys," doi: 10.1080/14786443209461944.
[61] Z. Jiao and G. S. Was, "Segregation behavior in proton- and heavy-ion-irradiated ferritic-martensitic alloys," *Acta Mater.*, vol. 59, no. 11, pp. 4467–4481, 2011, doi: 10.1016/j.actamat.2011.03.070.
[62] Z. Lu, R. G. Faulkner, G. Was, and B. D. Wirth, "Irradiation-induced grain boundary chromium microchemistry in high alloy ferritic steels," *Scr. Mater.*, vol. 58, no. 10, pp. 878–881, 2008, doi: 10.1016/j.scriptamat.2008.01.004.
[63] N. Yoshida, A. Yamaguchi, T. Muroga, Y. Miyamoto, and K. Kitajima, "Characteristics of point defects and their clustering in pure ferritic steels," *J. Nucl. Mater.*, vol. 155–157,

no. PART 2, pp. 1232–1236, 1988, doi: 10.1016/0022-3115(88)90502-8.
[64] E. Aydogan *et al.*, "α′ formation kinetics and radiation induced segregation in neutron irradiated 14YWT nanostructured ferritic alloys," *Sci. Rep.*, vol. 9, no. 1, pp. 1–12, 2019, doi: 10.1038/s41598-019-44508-5.